



Shadow-aware terrain correction for karst landforms using remote sensing data

Hongbo Yan, Qian Yu, Xianjian Lu, Jiahua Wang, Guoqing Zhou, Tianjie Zhao & Rao Liang

To cite this article: Hongbo Yan, Qian Yu, Xianjian Lu, Jiahua Wang, Guoqing Zhou, Tianjie Zhao & Rao Liang (2025) Shadow-aware terrain correction for karst landforms using remote sensing data, International Journal of Remote Sensing, 46:22, 8834-8855, DOI: [10.1080/01431161.2025.2573242](https://doi.org/10.1080/01431161.2025.2573242)

To link to this article: <https://doi.org/10.1080/01431161.2025.2573242>



Published online: 28 Oct 2025.



Submit your article to this journal [↗](#)



Article views: 24



View related articles [↗](#)



View Crossmark data [↗](#)



Shadow-aware terrain correction for karst landforms using remote sensing data

Hongbo Yan^a, Qian Yu^a, Xianjian Lu^a, Jiahua Wang^a, Guoqing Zhou^a,
Tianjie Zhao^b and Rao Liang^c

^aCollege of Geomatics and Geoinformation, Guilin University of Technology, Guilin, Guangxi, China; ^bState Key Laboratory of Remote Sensing Science, Aerospace Information Research Institute, Chinese Academy of Sciences, Beijing, Beijing, China; ^cGuangxi Zhuang Autonomous Region Natural Resources Investigation and Monitoring Institute, Nanning, Guangxi Zhuang Autonomous Region, China

ABSTRACT

Terrain correction is crucial in enhancing the quality of remote sensing imagery in mountainous regions by mitigating terrain-induced distortions. Despite advancements, current methods fall short in effectively addressing terrain shading issues. The Semi-empirical Method Considering Shadow (SMCS) was developed in this study, and the performance of SMCS, SCS, and SCS+C models on images of varying spatial resolution in karst landscapes was also evaluated. The results demonstrate that the SMCS method effectively enhances remote sensing images of complex mountainous areas. Compared with the traditional terrain correction method, the SMCS method significantly improves the correction effect. The R^2 , which reflects the relationship between solar incidence angle and image reflectance, decreased from 0.489, 0.037, and 0.067 to 0.046, 0.018, and 0.022, respectively. This indicates that the SMCS method effectively weakens the linear correlation between image reflectance and solar incidence angle. Additionally, the IQRR across bands confirms the SMCS method's ability to correct spectral discrepancies among similar features. The SMCS model demonstrates robust performance across all tested resolutions, confirming its broad applicability and effectiveness under varying spatial scales. Furthermore, the study highlights that terrain-induced effects become increasingly significant at higher resolutions, posing substantial challenges to conventional correction approaches.

ARTICLE HISTORY

Received 25 July 2025

Accepted 6 October 2025

KEYWORDS

SMCS method; terrain correction; karst landforms; high resolution

1. Introduction

Remote sensing imagery is an effective means of acquiring surface information that reflects the spectral, spatial, and structural characteristics of land objects (Hu et al. 2020; Wu et al. 2017). These characteristics are crucial for research in fields like geography, ecology, agriculture, and hydrology. However, the accuracy of spectral data is influenced by various factors, including atmospheric conditions, imaging technology, and sensor characteristics (Santini and Palombo 2022). Terrain is also a particularly significant factor, as uneven terrain results in differential solar radiation at different locations. This phenomenon manifests in

two distinct forms: ‘same body with different spectra’ and ‘different bodies with same spectrum’, such as self-shadow, cast shadow, and sunny areas, resulting from anisotropic solar illumination (H. Li et al. 2016; Nath and Ni-Meister 2021; Zhou et al. 2014). Terrain correction transforms pixel-level radiance or reflectance values from inclined terrain surfaces to a reference plane, typically horizontal, to eliminate terrain-induced illumination effects (M. Gao et al. 2015; M.-L. Gao et al. 2014). It is essential for improving the accuracy of change detection, land cover classification, post-drought vegetation recovery rate, and biophysical parameter retrieval. This correction is particularly critical in terrain-sensitive applications such as mangrove mapping, species-level classification, and recovery speed in response to extreme drought, where terrain effects can obscure subtle spectral differences (Fu et al. 2022; Lu et al. 2025; Yao et al. 2025). Nie et al. (2021) found that after terrain correction, the terrain effects on the Remote Sensing Ecological Index (RSEI) were significantly reduced, thereby enhancing its practical applicability. Therefore, terrain correction is fundamental for reducing terrain-related radiometric distortions and ensuring the consistency and reliability of remote sensing analyses.

To achieve more accurate surface reflectance, researchers have developed various terrain correction models, categorized into empirical, physical, and semi-empirical models (Lin et al. 2020; Y. Ma et al. 2021). Empirical models are based on statistical or regression analysis to establish a relationship between image reflectance and terrain factors, adjusting coefficients or weights to reduce terrain effects (Y. Gao and Zhang 2009; Richter, Kellenberger, and Kaufmann 2009). The primary advantage of this method is its simplicity, as it does not require complex parameter inputs; however, empirical models also have inherent limitations (Blesius and Weirich 2005; H. Li et al. 2016). These include a lack of a physical basis, an inability to truly reflect the reflectance characteristics of ground objects, and limitations imposed by specific image and terrain conditions. Consequently, they are difficult to apply broadly (Baraldi, Girona, and Simonetti 2010). Physical models, grounded in radiative transfer theory, establish complex physical relationships between the reflectance of remotely sensed imagery and factors like terrain, sunlight angle, observation angle, and atmospheric conditions. These models consider the Lambertian or non-Lambertian properties of surfaces when calculating the total radiation (Santini and Palombo 2019; Yin et al. 2018). These models recover the true reflectance of ground objects by calculating the total surface radiation, offering strong physical significance. However, physical models depend on high-precision terrain data and require numerous input parameters (Chen et al. 2023; A. Li et al. 2015). Their computational complexity and relatively low processing efficiency may limit their applicability, particularly in large-scale remote sensing image processing (Fan, Li, and Liu 2015).

To balance the physical basis of models with computational efficiency, researchers often use semi-empirical models. These models introduce empirical parameters with physical meaning, reduce the auxiliary data required for physical models, and minimize the reliance of empirical models on image data and experience. For example, Teillet, Guindon, and Goodenough (1982) incorporated an empirical coefficient c into the cosine correction model. This coefficient is calculated through a regression formula between the brightness of slope pixels and the cosine of the solar incidence angle. Liu et al. (2007) optimized the C correction parameters based on the empirical linear relationship between radiometric values and illumination coefficients, resulting in an approximately 16% improvement in reflectance fidelity over vegetated areas. Gu and

Gillespie (1998) proposed the SCS (Sun-Canopy-Sensor) correction model, which assumes that the illuminated canopy reflection is independent of the terrain, thus improving the correction accuracy on sunny slopes. Soenen, Peddle, and Coburn (2005) introduced the c parameter into the SCS model and developed the SCS+C model to address the overcorrection issue. The non-Lambertian method takes into account the spatial relationship between the sun and the sensor. The Minnaert model characterizes surface BRDF using a parameter k ($0 \leq k \leq 1$), and its adaptive adjustment capability ensures improved radiometric consistency in complex terrains such as plateaus and mountainous regions. Reeder (2002) proposed the Minnaert+SCS model, which builds on the correlation between the C correction parameter and the Minnaert constant k . However, its computational complexity limits its practical applicability. While semi-empirical models strike a balance between accuracy and efficiency, they often neglect the impact of terrain shadows in mountainous areas. For instance, while models such as Minnaert and SCS+C perform well in highland and mountainous regions, they still fall short in accurately handling shaded areas in complex terrains, such as basins and karstic terrains. These limitations constrain their applicability in complex terrains (Yan, Wang, and Lu 2023).

To address this issue, researchers have proposed shadow detection and correction methods based on vegetation indices (Z. Ma et al. 2020). For example, Zhang et al. (2024) proposed a triple shadow multilinear mixing model-based shadow removal method (triple-SMLM), which improves the accuracy of shadow removal in vegetated canopies. Similarly, Jiang, Chen, et al. (2022) proposed a shadow correction method based on the Shadow Elimination Vegetation Index (SEVI), using the consistency of SEVI in shaded and non-shaded areas to mitigate shadow effects. Although these methods are effective for single bands, they lack multispectral information, which is essential for comprehensively understanding and interpreting remote sensing data (Riano et al. 2003). Furthermore, these methods have not been fully validated with higher-resolution imagery (e.g. Sentinel-2 and GF-2) or in more complex and fragmented karst terrains, and their correction performance remains uncertain. Therefore, further research is necessary to enhance their applicability and accuracy in complex terrains and high-resolution remote sensing data.

Research indicates that the effect of terrain on image quality may vary at different resolutions. For example, Ling, Li, and Jin (2023) found that terrain's impact on the Leaf Area Index becomes more pronounced as spatial resolution increases. This finding highlights the lack of comprehensive and in-depth validation and comparison of existing models at different resolutions. This lack of validation limits our understanding of correction models and their effectiveness, impacting their broader applicability. Therefore, we will conduct a pioneering quantitative analysis of the impact of different image resolutions on terrain correction in karst landscapes.

Our contributions can be summarized as follows.

- (1) We develop a semi-empirical SMCS model that incorporates a shadow factor to account for shadow effects, addressing the limitations of traditional terrain correction models.
- (2) We conduct an in-depth comparative analysis of the effectiveness of various terrain correction methods, focusing on the evaluation of their performance under karst landscapes conditions.

- (3) We evaluated the adaptability and performance variations of these methods across different image resolutions, further emphasizing the superiority of the new model at each resolution.

2. Study area and data sets

2.1. Study area

The study area is Yangshuo County (Figure 1), located in the southeastern region of Guilin City, Guangxi Zhuang Autonomous Region, China (24°28′–25°04′N, 110°13′–110°40′E). This region is characterized by mountains, hills, and karst landforms, with scattered river alluvial plains. The area is characterized by a subtropical humid climate, with an average annual temperature of 16–20°C and annual precipitation of 1900–2000 mm. The vegetation primarily consists of evergreen and deciduous broadleaf forests, along with bamboo forests, all of which interact closely with the rugged terrain. There is a complex interaction between these vegetation conditions and the surrounding terrain. The region is characterized by highly fragmented terrain with sharp elevation differences, forming a typical karst landscape featuring isolated peaks, intersecting valleys, and a complex mosaic of peak-cluster depressions. This rugged topography, with frequent and abrupt slope variations, leads to substantial differences in solar radiation received across different slope aspects and orientations, resulting in complex illumination patterns and pronounced shadow effects. The diverse landscapes along the Li River and the karstic features of the limestone mountain ranges contribute to the complexity of the terrain, which presents challenges for terrain correction. These features include unique terrain effects and complex vegetation distribution, potentially leading to shading of mountain surfaces. The irregular terrain results in a highly diverse spatial distribution. These distinctive topographic features differ from typical mountainous terrain and may affect the effectiveness of terrain correction.

2.2. Data sets

This study used the atmospherically corrected surface reflectance dataset from the Landsat 8 OLI/TIRS sensor. The dataset has an image resolution of 30 metres and consists of five visible and near-infrared bands, two shortwave infrared bands, and two thermal infrared bands. To mitigate the effects of noise and cloud shadows, a median synthesis process was performed using image data with less than 10% cloud coverage from 2015 to 2019. This process calculates the median value of each pixel in all matching bands.

Furthermore, Sentinel-2 satellite imagery was utilized. This dataset comprises 13 bands, with the blue, green, red, and near-infrared bands offering a spatial resolution of 10 metres, thereby facilitating the acquisition of more detailed information on surface features.

Additionally, data from the GF-2 satellite, provided by the China Resources Satellite Application Centre, were used. The GF-2 satellite is equipped with two 2 m/8 m panchromatic/multispectral cameras and four 16 m wide-field multispectral cameras, covering the spectral range from visible to near-infrared. In this study, multispectral and panchromatic remote sensing images acquired by the GF-2 satellite in 2015 are employed.

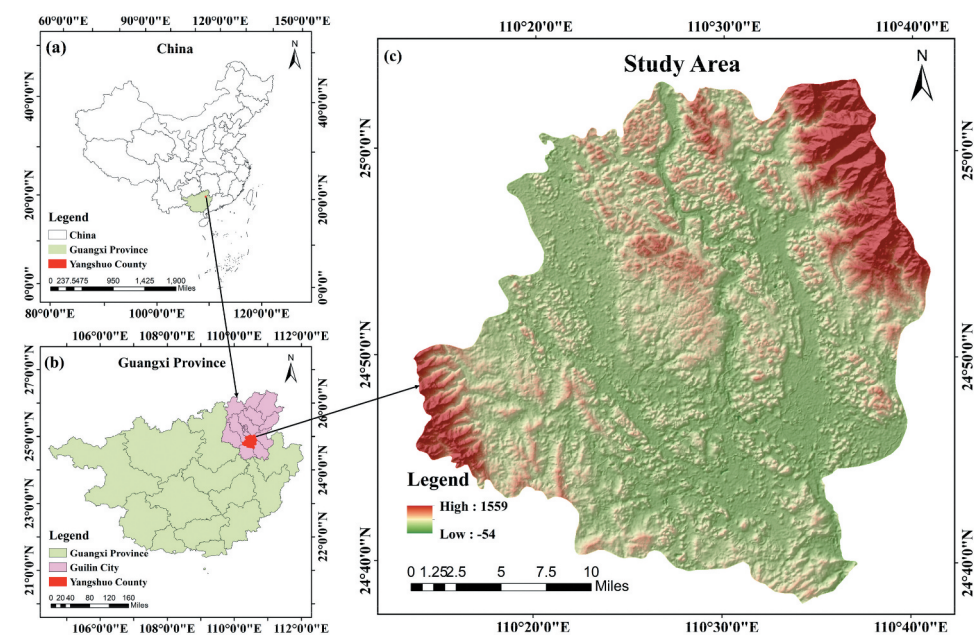


Figure 1. The study area; (a) represents the province where the study area is located and its approximate location in China; (b) indicates the specific location of the study area; (c) is the general overview map of the study area.

Table 1. Summary of data sources.

Variable name	Spatial resolution	Data source
Landsat 8	30m	https://earthexplorer.usgs.gov/ .
Sentinel-2	10m	https://sentinels.copernicus.eu/ .
GF-2	2m	https://www.cresda.com/ .
SRTM V3	30m	https://srtm.csi.cgiar.org/ .

The DEM data used are from the SRTM V3 product, which has a resolution of one arc second (30 metres). Sources of the data are shown in Table 1.

3. Methodology

The technical specifications, the improved model, and the validation methodology followed in this study are illustrated in Figure 2.

3.1. Traditional terrain correction models

The SCS model is designed to correct brightness variations in remote sensing images caused by terrain features, such as mountains. It estimates the influence of terrain using the DEM and adjusts the image pixels to reduce terrain-induced distortions. The SCS+C model improves upon the SCS by introducing a semi-empirical parameter C, which enhances the correction. However, traditional terrain correction models like the SCS and SCS+C models (Table 2) do not adequately address the impact of shadows.

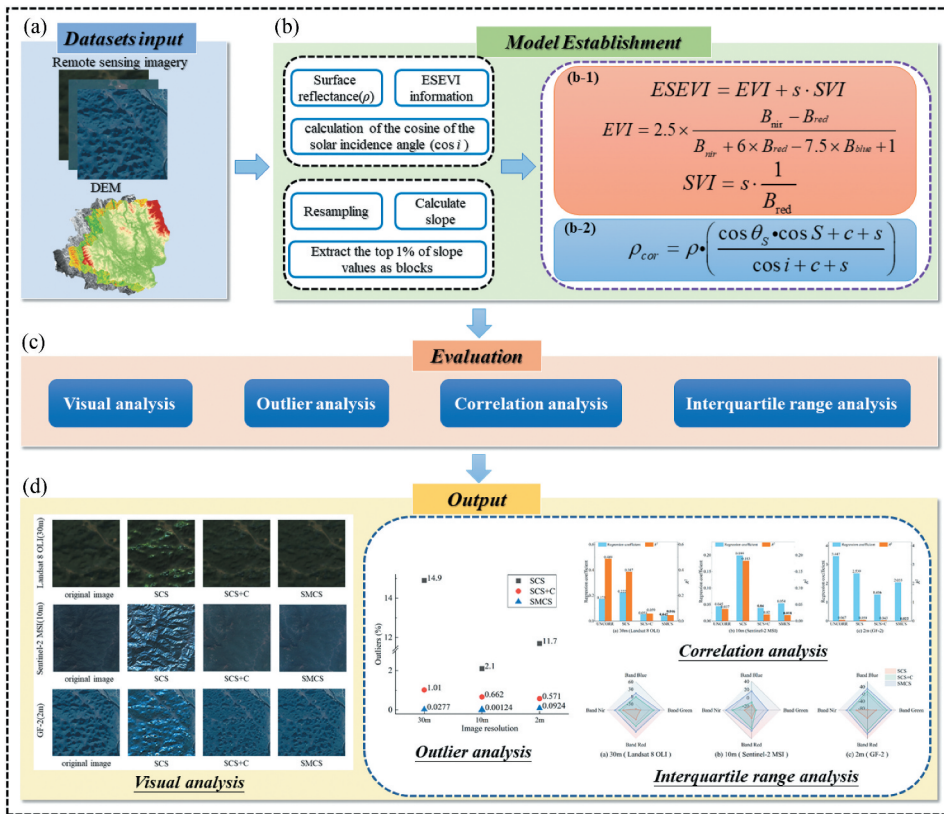


Figure 2. Establishment and evaluation process of the SMCS model: (a) input remote sensing imagery and DEM data; (b) process the remote sensing imagery and DEM data, and calculate the optimal adjustment factor (s) to establish the SMCS model; (c) evaluate the SMCS model; (d) output the correction results and verify the superiority of the model.

Table 2. Traditional terrain correction models.

Models	Formula	Presenter
SCS	$\rho_{cor} = \rho \left(\frac{\cos \theta_s \cos S}{\cos i} \right)$	Gu et al. (1998)
SCS+C	$\rho_{cor} = \rho \left(\frac{\cos \theta_s \cos S + c}{\cos i + c} \right)$	Soenen et al. (2005)

$$\cos i = \cos \theta_s \cdot \cos S + \sin \theta_s \cdot \sin S \cdot \cos(\varphi_a - \varphi_0) \quad (1)$$

$$\rho = a \cdot \cos i + b \quad (2)$$

Where ρ_{cor} is the terrain-corrected reflectance; ρ is the original reflectance of each pixel in the image; $\cos \theta_s$ is the cosine of the solar zenith angle; S is the slope of the terrain; $\cos i$ is the cosine of the solar incidence angle; c is an empirical parameter, where $c = b/a$, and a and b are the regression coefficients of the linear regression Formula between pixel reflectance and the cosine of the solar zenith angle; φ_a is the solar azimuth angle; φ_0 is the aspect of the terrain.

3.2. SMCS model establishment

In mountainous regions with complex and variable topography, the interpretation and extraction of remote sensing data are primarily affected by two types of shading: principal shadow and cast shadow. These shadow effects not only cause uneven radiation distribution in images but also complicate the accurate estimation of vegetation parameters. The challenge of terrain correction is further intensified by the elevation differences, vegetation complexity, and varying reflectance characteristics between the red and infrared bands compared to other features. In terrains with intricate landscapes, such as karst landforms, the shadow effect becomes even more pronounced due to frequent elevation changes and the extensive diversity of vegetation.

To address the challenges of shadow effects and overcorrection, this paper proposes the SMCS model, a semi-empirical terrain correction model that considers shadows. The SMCS model enhances and builds upon the SCS+C model, extending its capabilities. The optimal adjustment factor, derived from the calculation of the Enhanced Shadow Elimination Vegetation Index (ESEVI), is used as the shadow elimination factor 's'. This coefficient effectively mitigates the impact of shadows on terrain corrections, enhancing the elimination of terrain effects and optimizing the SCS+C model to create the SMCS model. The algorithm's formula is as follows:

$$\rho_{cor} = \rho \left(\frac{\cos \theta_s \cos S + c + s}{\cos i + c + s} \right) \quad (3)$$

Where 's' is the shadow elimination factor, derived from the ESEVI, which is a key parameter in determining the extent of shadow elimination.

3.3. Calculation of the parameter

The Shadow Elimination Vegetation Index (SEVI) is a tool designed to remove the influence of terrain shadows on vegetation reflectance Jiang et al. (2018). This index leverages the reflectance properties of the red and infrared bands to perform radiometric correction in shadowed areas, effectively removing shadow effects while preserving vegetation information in non-shadow areas. The red and infrared bands are particularly sensitive to vegetation information in remote sensing images. Vegetation typically exhibits higher reflectance compared to other land cover types, with vegetation on sunlit slopes showing higher reflectance than that on shaded slopes (Cochrane 2000). As terrain shading intensifies, its impact on the infrared band becomes more significant. Therefore, by applying the inverse function of red band reflectance to enhance the signal from shaded hillside vegetation and using the terrain shadow effect in the infrared band to suppress the signal from sunlit hillside vegetation, the SEVI formula is derived as follows:

$$SEVI = \frac{B_{nir}}{B_{red}} + f \cdot \frac{1}{B_{red}} = RVI + f \cdot SVI \quad (4)$$

Where B_{red} is the red-band reflectance of the image, B_{nir} is the infrared-band reflectance of the image, RVI is the ratio vegetation index, SVI is the shadow vegetation index, f is the adjustment factor.

Compared to the Ratio Vegetation Index (RVI), the Enhanced Vegetation Index (EVI) demonstrates significant advantages, particularly in complex environments, such as karst landscapes. Firstly, EVI demonstrates a greater degree of resistance to atmospheric and soil background interferences. The incorporation of an atmospheric correction parameter, designated as EVI , serves to mitigate the impact of atmospheric scattering and aerosols. Conversely, RVI, as a simplified vegetation index, is based solely on the ratio of red and near-infrared band reflectance, rendering it more susceptible to atmospheric variations, which limits its applicability in dynamic environments.

In karst landscapes, where terrain is highly undulating and vegetation density and coverage are typically high, traditional vegetation indices (e.g. RVI) often suffer from saturation. This saturation has been shown to distort vegetation signals in high-reflectance areas, thereby compromising the accuracy of vegetation change detection. This phenomenon not only impacts the extraction of vegetation information but also constrains the accuracy of the SEVI. To address this issue, the present study introduces the EVI in place of the RVI to refine the calculation of the shadow factor, and proposes the Enhanced Shadow Elimination Vegetation Index (ESEVI). This index not only improves the accuracy of shadow factor estimation but also expands the range of spectral band coverage, enabling more effective terrain correction. The ESEVI formula is derived as follows:

$$ESEVI = 2.5 \times \frac{B_{\text{nir}} - B_{\text{red}}}{B_{\text{nir}} + 6 \times B_{\text{red}} - 7.5 \times B_{\text{blue}} + 1} + s \cdot \frac{1}{B_{\text{red}}} = EVI + s \cdot SVI \quad (5)$$

Where B_{red} is the red-band reflectance of the image, B_{nir} is the infrared-band reflectance of the image, B_{blue} is the blue-band reflectance of the image, EVI is the enhanced vegetation index, SVI is the shadow vegetation index, and s is the key parameter to determine the degree of shadow elimination.

The key parameter ' s ' is a pivotal element in determining the extent of shadow elimination. It adjusts the balance between under- and over-elimination of topographic shadows in rugged terrain. The block information entropy (BIE) algorithm, based on information entropy theory, is employed to calculate the adjustment factor (Jiang, Chen, et al. 2022). In cases where vegetation is uniformly distributed across rugged terrain, removing terrain-induced effects leads to an increase in the information entropy of ESEVI. The optimal value of the adjustment factor ' s ' can be identified when the information entropy reaches its maximum.

$$\ln f = - \frac{\sum_{i=1}^n p_i \ln(p_i)}{\ln(n)} \quad (6)$$

$$p_i = \frac{x_i}{\sum_{i=1}^n x_i} \quad (7)$$

$$\sum_{i=1}^n p_i = 1, 0 < p_i < 1 \quad (8)$$

$$s_l = \arg \max(\ln f), s \in (0.001, 1.000) \quad (9)$$

$$s_w = \arg \max(\ln f_1), s \in (s_u, j = 1, \dots, m) \quad (10)$$

Where $\ln f$ is the information entropy of the ESEVI in the block, p_i is the percentage of the ESEVI value of the pixels in the selected block, x_i is the pixel value of the ESEVI, n is the number of pixels in the selected block, s_l is the optimization adjustment factor of the block, s_w is the optimal adjustment factor for the whole scene, $\ln f_1$ is the maximum information entropy of the ESEVI in the block, and m is the number of the selected blocks in the whole scene image.

3.4. Outlier analysis

The outlier ratio quantifies the proportion of an image containing pixels with corrected surface reflectance values that fall outside the range of the original image's surface reflectance (Hantson and Chuvieco 2011). In other words, it measures the extent to which the corrected reflectance exceeds the maximum or falls below the minimum of the original reflectance. A higher outlier ratio indicates poorer terrain correction quality (Altuntas, Erdogan, and Tunalioglu 2024; Dozier et al. 2022).

3.5. Correlation analysis

To evaluate the effectiveness of terrain correction, one of the most commonly used methods is to analyse the correlation between surface reflectance and the cosine of solar incidence. Terrain correction should theoretically reduce the linear correlation between these two variables in the original image (Bishop et al. 2019). In this study, a linear regression analysis is applied to compare the surface reflectance and cosine of solar incidence before and after correction. The slope of the linear regression formula indicates the strength of the correlation; a larger slope suggests a stronger terrain effect. The quality of the regression results can be assessed by determining the coefficient of determination, R^2 , which indicates how well the regression formula fits the data (Formula 11) (Chen et al. 2023).

$$R^2 = 1 - \frac{\sum_i (y_i - \hat{y}_i)^2}{\sum_i (y_i - \bar{y}_i)^2} \quad (11)$$

where y_i is the pixel reflectance, \hat{y}_i is the predicted value of the reflectance obtained by linear fitting, and \bar{y}_i is the average value of the reflectance. The value of R^2 varies between 0 and 1 and can be used to quantify the terrain effect in the image after terrain correction. In general, the smaller the corrected R^2 , the better the correction, as it indicates that the terrain correction has reduced the linear correlation between the surface reflectance and the cosine of solar incidence; conversely, the larger the

corrected R^2 , the worse the correction, as it indicates that there is still a strong linear correlation between the surface reflectance and cosine of solar incidence, i.e. there is still a significant terrain effect in the image. Consequently, the efficacy of terrain correction can be evaluated by contrasting the R^2 before and after correction.

3.6. Statistical analysis

Statistical analysis methods evaluate calibration effectiveness by analysing spectral variations across different bands before and after calibration or by examining variations in surface cover types. The assessment of surface reflectance fluctuations typically involves the utilization of metrics, such as mean values and standard deviations.

3.7. Interquartile range analysis

The interquartile range reduction rate (IQRR) is a crucial metric for evaluating the effectiveness of terrain correction by measuring how much the interquartile range (IQR) is reduced after correction. The IQR, which represents the difference between the upper quartile (Q3) and lower quartile (Q1) of the image data, reflects the extent of spectral variation among similar objects in the image. A smaller IQR value indicates less spectral difference between these objects (Richter, Kellenberger, and Kaufmann 2009). Therefore, when the *IQRR* increases, it indicates that the terrain correction improves the image quality, i.e. the terrain correction reduces the spectral differences between similar objects (Formula 12). By analysing the IQRR, one can assess the spectral consistency of similar objects in the corrected image, which in turn reflects the spatial distribution characteristics of surface reflectance.

$$IQRR = 100 \cdot 1 - \frac{IQR_{corr,\lambda}}{IQR_{\lambda}} \quad (12)$$

Where *IQRR* is the interquartile range reduction, and IQR_{λ} and $IQR_{corr,\lambda}$ are the interquartile ranges of each band before and after correction. The IQRR reflects the degree of change in the spectral difference of similar objects in the corrected image; the larger the IQRR, the smaller the corrected interquartile range, indicating that the correction effect is better; the smaller the IQRR, the larger the corrected interquartile range, indicating that the correction effect is worse; and a negative IQRR value indicates that the corrected interquartile range increases, indicating that the correction effect is worse.

4. Results

4.1. Terrain correction results and visual analysis

Terrain correction experiments were conducted on three images with different resolutions from the Yangshuo study area, employing three correction models: SCS, SCS+C, and SMCS. The images were comprehensively evaluated using various assessment indices. Figure 3 illustrates the comparative analysis of the images at different resolutions, both before and after correction using different methodologies.

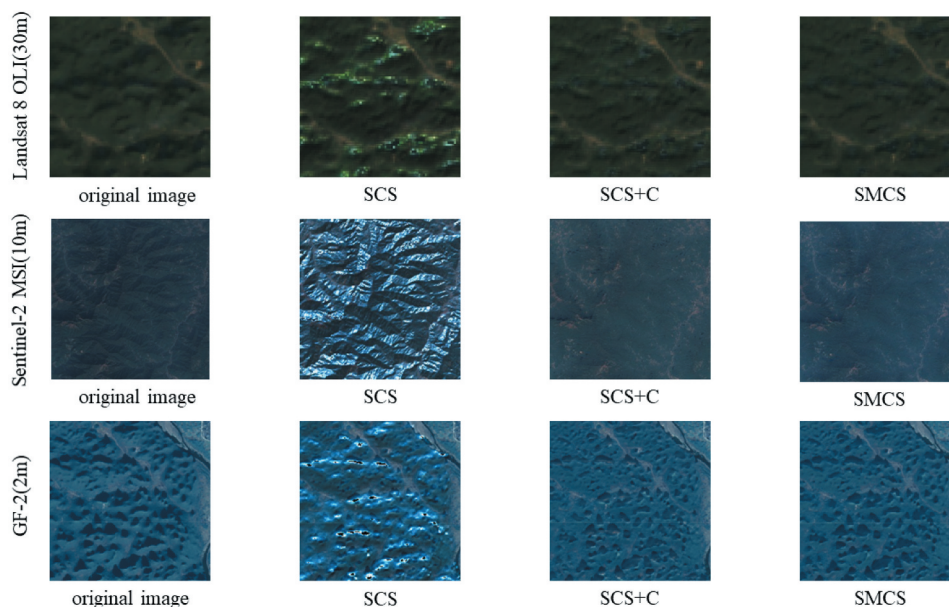


Figure 3. Comparing images of different resolution before and after correction using different methods.

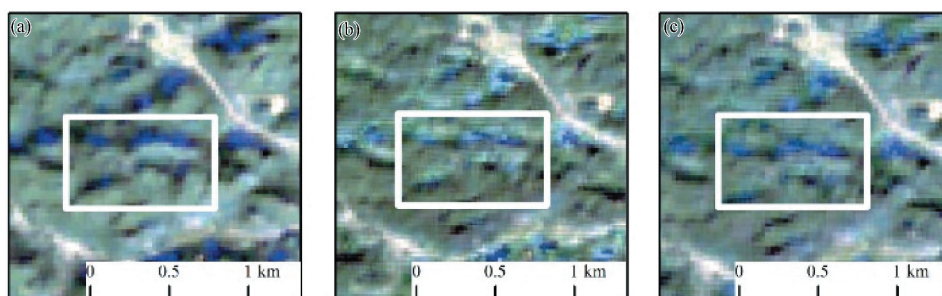


Figure 4. Terrain correction in the Landsat 8 OLI image: (a) original image; (b) image corrected by SCS+C model; (c) image corrected by SMCS model.

Terrain relief significantly affects pixel brightness, with sunny slopes appearing much brighter than shaded slopes, leading to visible terrain shadows. The SCS model often results in excessive brightness and distortion in shadowed areas of rugged mountain images. Although the SCS+C model improves upon this by reducing some of the over-brightness and distortion, it still tends to overcorrect shadow regions. In contrast, the SMCS model excels at minimizing both overbrightness and distortion, producing a more uniform colour tone and better overall image correction.

In the Landsat 8 OLI image (Figure 4), the SCS+C model enhanced reflectivity in shadowed areas and achieved a more consistent image tone, but it still overcorrected some shadow regions. In contrast, the SMCS model effectively removed the overbright pixels in these shadowed areas, providing a more balanced correction.

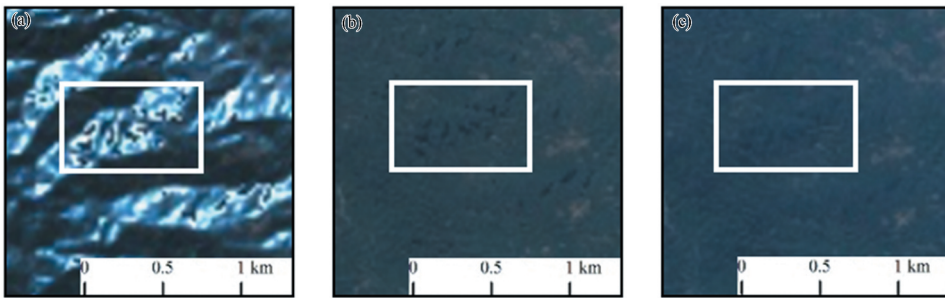


Figure 5. Terrain correction in the Sentinel-2 MSI image: (a) original image; (b) image corrected by SCS +C model; (c) image corrected by SMCS model.

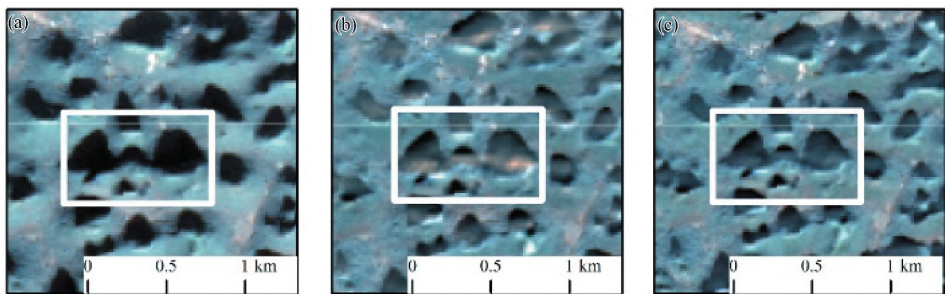


Figure 6. Terrain correction in the GF-2 image: (a) original image; (b) image corrected by SCS+C model; (c) image corrected by SMCS model.

In the Sentinel-2 MSI image (Figure 5), the SCS model noticeably enhanced terrain effects, while the SCS+C and SMCS models effectively reduced the influence of terrain. However, the SCS+C model exhibited signs of overcorrection within the white box area, indicating that the SMCS model provides superior correction performance.

In the GF-2 image (Figure 6), the SCS+C model improved reflectivity and detail in shadowed areas but also caused overcorrection in these regions. In contrast, the SMCS model effectively addressed the overcorrection issue observed with the SCS+C model, leading to more accurate results.

In summary, the SMCS model has been demonstrated to effectively correct for the topographical effects of karst landforms in images of different resolutions.

4.2. Outlier analysis

Outliers are surface reflectance values that deviate from the maximum or minimum values of the original image. The outlier ratio represents the proportion of these outliers relative to the entire image. Studies have demonstrated that the quality of terrain correction is strongly correlated with the outlier ratio. Therefore, lower-quality terrain correction methods typically lead to higher outlier ratios. Figure 7 presents the changes in outlier ratios for three different terrain correction methods (SCS, SCS+C and SMCS) across varying resolutions (30 m, 10 m, 2 m).

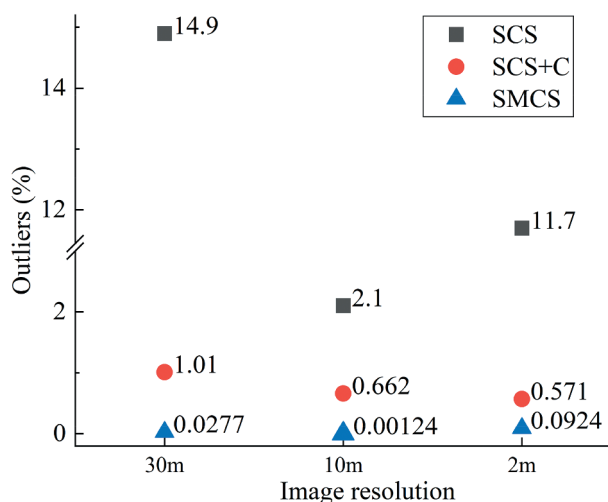


Figure 7. The percentage of outliers in images of different resolutions corrected by different models.

The results of the outlier analysis reveal that images corrected using the SCS+C and SMCS models have significantly lower outlier ratios than those corrected with the SCS model. This suggests that both the SCS+C and SMCS models better account for the geotropic growth patterns of trees and the effects of scattered radiation, thereby improving correction accuracy. The SMCS model, in particular, consistently shows the lowest outlier ratios across all resolutions, highlighting its superior effectiveness in terrain correction.

4.3. Correlation analysis

In this study, the linear correlation between reflectance and the cosine of the solar incidence angle was used as a metric to assess the effectiveness of terrain correction. The goal of terrain correction is to mitigate the impact of terrain on image reflectance, thereby reducing this linear correlation. Linear regression analysis, based on Formula 11, was performed to compare the relationship between reflectance and the cosine of the solar incidence angle before and after correction using different terrain correction methods at various resolutions (Figure 8).

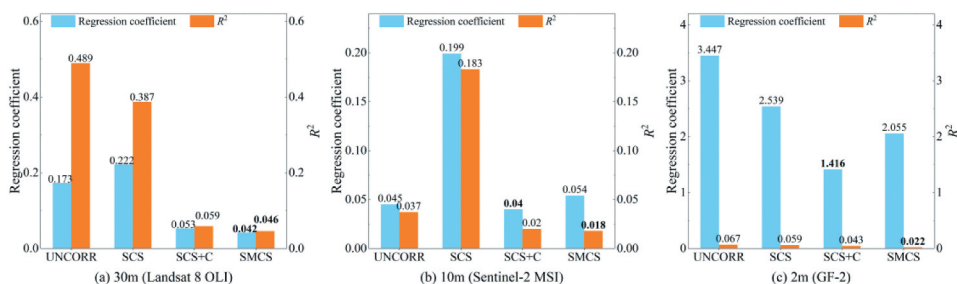


Figure 8. Linear regressions slopes and coefficients of determination after correction by different methods: (a) 30m resolution (Landsat 8 OLI); (b) 10m resolution (Sentinel-2 MSI); (c) 2m resolution (GF-2).

The results of the correlation analysis demonstrate that different terrain correction methods significantly influence the relationship between reflectance and the cosine of the solar incidence angle at various resolutions. In the Landsat 8 OLI imagery, the original image exhibited a strong linear correlation between reflectance and the cosine of the solar incidence angle, with a slope of 0.173 and an R^2 of 0.489. Following the SCS correction, this linear correlation was not effectively mitigated, as indicated by the increased slope of 0.222 and a reduced R^2 of 0.387. Conversely, the SCS+C and SMCS correction methods significantly reduced this linear correlation, with slopes decreasing to 0.053 and 0.042, respectively, and R^2 values dropping to 0.059 and 0.046. These findings indicate that both the SCS+C and SMCS methods effectively mitigate terrain effects. However, the SMCS model demonstrates the lowest R^2 and the most significant reduction, suggesting superior calibration performance. In summary, the SMCS method has been demonstrated to exhibit optimal calibration effectiveness.

In the Sentinel-2 MSI imagery, a notable linear correlation between reflectance and the cosine of the solar incidence angle, as shown by increases in both slope and R^2 . However, the SCS+C and SMCS corrections substantially reduced this linear correlation, leading to decreases in both slope and R^2 , with R^2 decreasing from 0.037 to 0.02 and 0.018, respectively. This demonstrates the effectiveness of these correction methods in mitigating terrain effects. Furthermore, the SMCS model demonstrates the lowest R^2 and the most substantial decline, indicating that after correction using the SMCS model, the image reflectance is closer to the true reflectance of the ground objects.

In the GF-2 imagery, the original R^2 was 0.067, indicating a weak linear correlation between reflectance and the cosine of the solar incidence angle. This may be attributed to the complex terrain in the study area, where steep rocky hills and mountain peaks contribute to the uneven radiation from adjacent terrains, thus increasing the difficulty of terrain correction in high-resolution imagery. Nevertheless, all terrain correction methods effectively reduced the linear correlation between reflectance and the cosine of the solar incidence angle. The SMCS correction method exhibited the lowest R^2 of 0.022, demonstrating its highest effectiveness in mitigating terrain effects.

Although the SCS+C model also yields low R^2 values across the three resolution images, the SMCS model further reduced these R^2 values by 22%, 10%, and 46.8%, respectively. This outcome serves to underscore the considerable advantage of the SMCS model in terms of its efficacy in correction performance across a range of resolution imagery. In summary, high-resolution imagery, such as Sentinel-2 MSI and GF-2, presents greater challenges for terrain correction due to more pronounced terrain effects. However, the SMCS method consistently offers superior correction performance across all resolutions, highlighting its effectiveness and reliability in addressing these terrain challenges.

4.4. Statistical analysis

To analyse the impact of different terrain correction models on the reflectance of different bands in remotely sensed images at different resolutions, this paper performed a statistical analysis of the reflectance parameters for each band at three image resolutions. The mean and standard deviation of reflectance were calculated for each image before and after the corrections were applied (Table 3).

Table 3. Statistics of surface reflectance of each image before and after correction.

		Blue		Green		Red		Nir	
		Mean	SD	Mean	SD	Mean	SD	Mean	SD
Landsat 8 OLI	Uncor	0.0387	0.0134	0.0595	0.0165	0.0496	0.0208	0.2291	0.0605
	SCS	0.0406	0.0177	0.0624	0.0226	0.0515	0.0228	0.2390	0.0753
	SCS+C	0.0388	0.0130	0.0596	0.0160	0.0497	0.0203	0.2289	0.0504
Sentinel-2 MSI	SMCS	0.0385	<u>0.0134</u>	0.0593	0.0158	0.0493	0.0202	0.2262	0.0492
	Uncor	0.1166	0.0107	0.1053	0.0120	0.0790	0.0207	0.2701	0.0383
	SCS	0.1147	1.4211	0.1030	1.2376	0.0776	0.7966	0.2621	3.3093
GF-2	SCS+C	0.1269	0.0104	0.1173	0.0106	0.0806	0.0191	0.2784	0.0320
	SMCS	0.1304	0.0097	0.1355	<u>0.0110</u>	0.0893	0.0185	0.2775	0.0256
	Uncor	3.8380	0.6200	2.9207	0.6659	1.8612	0.5772	3.7193	1.5609
	SCS	4.3209	11.1008	3.2141	7.4090	2.0082	4.1189	3.8147	5.5284
	SCS+C	3.8468	0.5854	2.9223	0.5351	1.8582	0.4940	3.6588	1.1833
	SMCS	3.8585	0.4701	2.9400	0.5045	1.8802	0.4699	3.7062	1.2959

A detailed analysis of Table 3 reveals significant shifts in reflectance across different image resolutions, both before and after correction. Initially, the mean reflectance values for each band were lower but increased following correction. Concurrently, the standard deviation decreases, indicating an effective reduction of terrain effects and a decrease in data variability. Notably, post-correction reflectance in the near-infrared band consistently surpassed that of other bands at all resolutions, likely due to its greater sensitivity to vegetation, which typically exhibits higher reflectance. Although the SCS+C model exhibits a slight advantage in minimizing standard deviation within certain single bands, overall, the SMCS model demonstrates the most outstanding performance in minimizing multi-band standard deviation across the three resolutions studied, fully reflecting its powerful effectiveness in reducing data variability.

However, the SCS model’s application to Sentinel-2 MSI (10 m) and GF-2 (2 m) data demonstrates its limitations in high-resolution imagery. For GF-2 (2 m) data, the discrepancies in reflectance after applying various correction models were less pronounced compared to the other resolutions. This is due to the finer spatial details captured by GF-2’s high-resolution imagery, which reduce the observable impacts of terrain correction.

4.5. Interquartile range analysis

To evaluate the impact of three terrain correction models (SMCS, SCS, and SCS+C) on image quality at three distinct resolutions (Landsat 8 OLI, Sentinel-2 MSI, and GF-2), we calculated the IQRR for specific image bands using formula (12). Figure 9 illustrates the

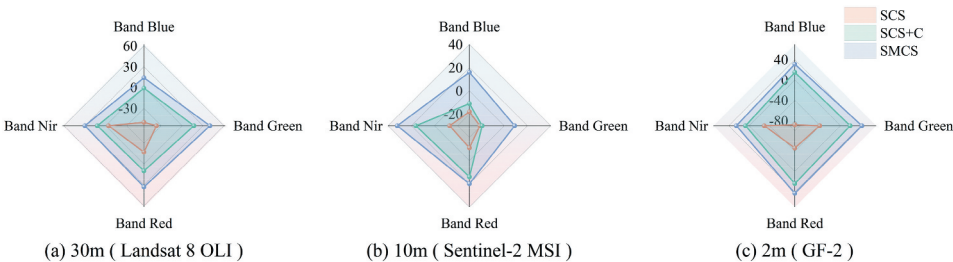


Figure 9. Reductions in interquartile ranges of each band after correction by different methods: (a) 30m resolution (Landsat 8 OLI); (b) 10m resolution (Sentinel-2 MSI); (c) 2m resolution (GF-2).

IQRR for specific bands (blue, green, red, and near-infrared) following the application of distinct correction models. The IQRR metric reflects the degree of spectral difference for the same type of ground objects across different bands. A higher IQRR indicates more effective terrain correction.

The results revealed that, for Landsat 8 OLI images, the SMCS method substantially mitigates spectral variations among analogous objects across all bands, with IQRR values of 14%, 40%, 33%, and 30%, respectively, substantially higher than those of the SCS and SCS+C methods. Notably, the green band showed a significant IQRR improvement of 40% with the SMCS method. In contrast, the SCS method exhibited negative IQRR values across all bands, while the SCS+C method also displayed a negative IQRR specifically in the blue band.

In Sentinel-2 MSI images, the SMCS method demonstrated the most optimal spectral adjustment outcomes across all bands, with IQRR values of 16%, 9%, 20%, and 32%, respectively. The adjustment performance was most prominent in the near-infrared band, where IQRR reached 32%. This finding suggests that the method effectively mitigated the impact of terrain effects while preserving the spectral characteristics of ground objects. In contrast, the SCS+C method exhibited IQRR values of -11% and -19% in the green and blue bands, respectively, reflecting its relatively weaker adjustment capability in these bands.

In the GF-2 image, the SMCS method continues to demonstrate outstanding spectral adjustment performance, with IQRR values of 31%, 42%, 43%, and 25%, respectively, all surpassing those of the SCS and SCS+C models. This finding suggests that the SMCS method can effectively suppress terrain effects at high resolutions while maintaining spectral consistency of land surfaces.

In summary, the SMCS method demonstrated robust spectral adjustment capabilities at various resolutions, effectively minimizing the spectral discrepancies between analogous features.

5. Discussion

In this paper, a terrain correction model, the SMCS model, which has been demonstrated to effectively mitigate the impact of shadows, is proposed. A systematic series of experiments are conducted in the study area, which features karst landforms with broken terrain and dramatic undulations, in conjunction with multi-resolution images. A comparison of the SMCS model with the traditional SCS and SCS+C models reveals significant advantages in terrain correction, particularly in terms of enhancing image quality and adjusting spectral information. Visual analysis showed that images corrected with the SMCS model exhibited uniform colour tones, sharp details, and reduced terrain shadows and spectral distortions. Furthermore, correlation analysis further revealed that the SMCS model effectively decreased the linear relationship between image reflectance and the cosine of the solar incidence angle, enhancing comparability. Statistical analysis demonstrated a significant reduction in outlier proportions with the SMCS model, leading to increased image accuracy. Additionally, the IQR analysis confirmed that the SMCS model was effective in reducing spectral differences between similar features.

In the Landsat 8 image, a significant difference in R^2 values is observed before and after applying terrain correction, with the SCS+C and SMCS models being particularly effective. This improvement can be attributed to the incorporation of the semi-empirical 'C' coefficient in both models, which substantially enhances correction performance (Chen et al. 2023). Additionally, the SMCS model further enhances performance by including the shading factor 's', which amplifies the correction's impact, especially in shadowed areas. Compared with the R^2 of the Sentinel-2 MSI and GF-2 images, the R^2 of the Landsat 8 impact decreases significantly. The reason for this may be due to the fact that the higher the resolution the more visible the surface details are, thus affecting the correction.

The impact of terrain effects varies with image resolution, with higher-resolution images often exhibiting more pronounced terrain effects due to increased surface detail (Chen et al. 2020; Deng et al. 2007; Zhu et al. 2013). For 30 m resolution images, there is a strong linear correlation between the original image's reflectance and the cosine of the solar incidence angle, indicating significant terrain effects. However, this correlation diminishes at resolutions of 10 m and 2 m. This discrepancy is likely due to complex terrain features, such as steep mountains and karst peaks, which cause uneven radiation across adjacent areas, making terrain correction more challenging for high-resolution images. In these images, the abundance of detailed ground features and the complexity of the terrain complicate parameter estimation and model fitting for terrain correction (Belgiu and Drăguț 2014). Therefore, improving the accuracy and effectiveness of terrain correction for high-resolution images requires a comprehensive consideration of multiple influencing factors.

The SMCS method excelled in correcting both shaded and non-shaded regions, effectively avoiding overcorrection. Moreover, it demonstrated superior correction performance across various resolutions, underscoring its adaptability and broad applicability. In contrast, the correction effects of the SCS and SCS+C models varied with different resolutions, indicating that these two methods were more sensitive to the characteristics and resolution of the image. In addition, the adjustment factor 's' in the SMCS method functions not just as a static value but as a mechanism for dynamically adjusting model parameters. This dynamic adaptation allows the SMCS method to effectively accommodate different resolution, terrain, and vegetation conditions, enhancing its flexibility and adaptability. Accordingly, the SMCS model introduces a highly promising dynamic moderator that demonstrates considerable potential in consideration of scale effects.

In addition, the variation in outlier ratio offers meaningful information for the analysis of scale effects. With increasing spatial resolution, the outlier ratio generally decreases, suggesting that high-resolution imagery tends to be more robust against scale-induced variability. This observation is consistent with the relationship between image resolution and surface detail representation, where higher-resolution data more accurately capture surface heterogeneity, thereby reducing reflectance deviations caused by terrain or other environmental factors. Furthermore, the SMCS model consistently achieved lower outlier ratios across all resolutions, indicating its superior capability in reducing spectral discrepancies among similar land cover types. These results demonstrate that the SMCS model not only effectively suppresses terrain-induced distortions but also maintains spectral integrity, thereby enhancing the overall spectral consistency of the corrected imagery.

In summary, the SMCS method demonstrates notable proficiency in the terrain correction of multi-resolution imagery, particularly in typical karst regions, exhibiting

commendable adaptability and stability. This study addresses the paucity of validation of analogous models in high-resolution images (e.g. Sentinel-2 and GF-2) and significantly reduces the uncertainty of terrain correction under karst landscapes conditions. The SMCS model provides a more reliable technical solution and new ideas for the optimization and application of subsequent models.

6. Conclusions

A Semi-Empirical Terrain Correction Model Considering Shadow Effects, called the SMCS method, was proposed in this paper, which includes a shading adjustment factor 's' based on the SCS+C model, improving efficiency in handling shading and terrain effects in rugged mountains. In addition, the method was validated using different resolutions optical imagery, investigating the impact of scale effects on terrain correction results. This study addresses the research gap in different scales terrain correction for complex karst landscapes. The SMCS, SCS, and SCS+C models were applied to the terrain correction of the study area at different resolutions. Various evaluation methods are used to compare and analyse the correction effects of these models at different resolutions. The experimental results show that:

- (1) The SMCS model exhibits the lowest outlier ratios across all resolutions compared to the traditional SCS and SCS+C models, thereby demonstrating its superior performance in terrain correction.
- (2) The R^2 of the images that were corrected using the SMCS model decreased significantly and was lower than that of the SCS and SCS+C models. For Landsat 8 OLI images, the R^2 decreased from 0.489 to 0.046. Similarly, the R^2 of the Sentinel-2 MSI images exhibited a decline, from 0.037 to 0.018. The GF-2 images demonstrated a comparable trend, with a decrease from 0.067 to 0.022. These findings indicate that the SMCS method is effective in reducing the reflectivity of images in a manner that is linearly correlated with the solar incidence angle.
- (3) Following the implementation of the SMCS model correction, there was an enhancement in the IQRR of images at varying resolutions. In comparison to the negative values observed in the SCS and SCS+C models, this finding indicates that the method is more effective at reducing spectral differences among similar objects and demonstrates strong spectral adjustment capabilities.
- (4) The SMCS method has been demonstrated to markedly enhance the quality of images with different resolutions, thereby substantiating its versatility for terrain correction at different resolutions.

In summary, in karst regions characterized by rugged and fragmented terrain, the SMCS model has been shown to eliminate the terrain and shadow effects while preserving the spectral characteristics of the features and enhancing the spectral consistency of the images. The SMCS method demonstrates remarkable improvement in image quality across different resolutions, with performance significantly surpassing that of traditional terrain correction models. Furthermore, we also demonstrate that the terrain correction performance of different models exhibits significant variation across spatial resolutions. The primary benefit of the SMCS

model is its capacity for flexible adjustment of terrain correction coefficients, enabling adaptation to diverse terrains, varying resolution imagery, and a range of vegetation conditions. This adaptability facilitates more precise characterization of the spectral characteristics of shaded areas. In the future, we will continue to advance terrain correction methodologies, focusing on the adaptability of the SMCS model across diverse geographic regions and investigating the impact of scale effects on correction accuracy. Concurrently, we will pursue improvements and innovations in terrain correction models to enhance precision and strengthen their applicability in complex environmental monitoring tasks.

Disclosure statement

No potential conflict of interest was reported by the author(s).

Funding

This paper is financially supported by Guangxi Natural Science Foundation under grant number [2025GXNSFAA069733], the Natural Science Foundation of China under Grant numbers [42361052], and Guangxi Key Laboratory of Automatic Detecting Technology and Instruments Program (Guilin University of Electronic Technology) [Contract number: YQ24202], ‘Guangxi Thousand Young and Middle-aged Backbone Teachers Cultivation Program for Colleges and Universities’ (Grant No. GuiJiao [2022]60).

ORCID

Hongbo Yan  <http://orcid.org/0000-0003-4090-0735>

Xianjian Lu  <http://orcid.org/0000-0002-1964-3765>

Data availability statement

The data that support the findings of this study are available from the corresponding author upon reasonable request

References

- Altuntas, C., B. Erdogan, and N. Tunalıoglu. 2024. “Implementing Robust Outlier Detection to Enhance Estimation Accuracy of GNSS-IR Based Seasonal Snow Depth Retrievals.” *International Journal of Remote Sensing* 45 (11): 3648–3663. <https://doi.org/10.1080/01431161.2024.2349265>.
- Baraldi, A., M. Gironde, and D. Simonetti. 2010. “Operational Two-Stage Stratified Topographic Correction of Spaceborne Multispectral Imagery Employing an Automatic Spectral-Rule-Based Decision-Tree Preliminary Classifier.” *IEEE Transactions on Geoscience & Remote Sensing* 48 (1): 112–146. <https://doi.org/10.1109/TGRS.2009.2028017>.
- Belgiu, M., and L. Drăguț. 2014. “Comparing Supervised and Unsupervised Multiresolution Segmentation Approaches for Extracting Buildings from Very High Resolution Imagery.” *ISPRS Journal of Photogrammetry & Remote Sensing* 96:67–75. <https://doi.org/10.1016/j.isprsjprs.2014.07.002>.
- Bishop, M. P., B. W. Young, J. D. Colby, R. Furfaro, E. Schiassi, and Z. Chi. 2019. “Theoretical Evaluation of Anisotropic Reflectance Correction Approaches for Addressing Multi-Scale Topographic Effects

- on the Radiation-Transfer Cascade in Mountain Environments." *Remote Sensing* 11 (23): 2728. <https://doi.org/10.3390/rs11232728>.
- Blesius, L., and F. Weirich. 2005. "The Use of the Minnaert Correction for Land-Cover Classification in Mountainous Terrain." *International Journal of Remote Sensing* 26 (17): 3831–3851. <https://doi.org/10.1080/01431160500104194>.
- Chen, R., G. Yin, G. Liu, J. Li, and A. Verger. 2020. "Evaluation and Normalization of Topographic Effects on Vegetation Indices." *Remote Sensing* 12 (14): 2290. <https://doi.org/10.3390/rs12142290>.
- Chen, R., G. Yin, W. Zhao, K. Yan, S. Wu, D. Hao, and G. Liu. 2023. "Topographic Correction of Optical Remote Sensing Images in Mountainous Areas: A Systematic Review." *IEEE Geoscience and Remote Sensing Magazine* 11 (4): 125–145. <https://doi.org/10.1109/MGRS.2023.3311100>.
- Cochrane, M. A. 2000. "Using Vegetation Reflectance Variability for Species Level Classification of Hyperspectral Data." *International Journal of Remote Sensing* 21 (10): 2075–2087. <https://doi.org/10.1080/01431160050021303>.
- Deng, Y., X. Chen, E. Chuvieco, T. Warner, and J. P. Wilson. 2007. "Multi-Scale Linkages Between Topographic Attributes and Vegetation Indices in a Mountainous Landscape." *Remote Sensing of Environment* 111 (1): 122–134. <https://doi.org/10.1016/j.rse.2007.03.016>.
- Dozier, J., E. H. Bair, L. Baskaran, P. G. Brodrick, N. Carmon, R. F. Kokaly, C. E. Miller, K. R. Miner, T. H. Painter, and D. R. Thompson. 2022. "Error and Uncertainty Degrade Topographic Corrections of Remotely Sensed Data." *Journal of Geophysical Research Biogeosciences* 127 (11): e2022JG007147. <https://doi.org/10.1029/2022JG007147>.
- Fan, W., J. Li, and Q. Liu. 2015. "GOST2: The Improvement of the Canopy Reflectance Model GOST in Separating the Sunlit and Shaded Leaves." *IEEE Journal of Selected Topics in Applied Earth Observations & Remote Sensing* 8 (4): 1423–1431. <https://doi.org/10.1109/JSTARS.2015.2413994>.
- Fu, B., X. He, H. Yao, Y. Liang, T. Deng, H. He, D. Fan, G. Lan, and W. He. 2022. "Comparison of RFE-DL and Stacking Ensemble Learning Algorithms for Classifying Mangrove Species on UAV Multispectral Images." *International Journal of Applied Earth Observation and Geoinformation* 112:102890. <https://doi.org/10.1016/j.jag.2022.102890>.
- Gao, M., H. Gong, W. Zhao, B. Chen, Z. Chen, and M. Shi. 2015. "An Improved Topographic Correction Model Based on Minnaert." *GIScience and Remote Sensing* 53 (2): 247–264. <https://doi.org/10.1080/15481603.2015.1118976>.
- Gao, M.-L., W.-J. Zhao, Z.-N. Gong, H.-L. Gong, Z. Chen, and X.-M. Tang. 2014. "Topographic Correction of ZY-3 Satellite Images and Its Effects on Estimation of Shrub Leaf Biomass in Mountainous Areas." *Remote Sensing* 6 (4): 2745–2764. <https://doi.org/10.3390/rs6042745>.
- Gao, Y., and W. Zhang. 2009. "A Simple Empirical Topographic Correction Method for ETM+ Imagery." *International Journal of Remote Sensing* 30 (9): 2259–2275. <https://doi.org/10.1080/01431160802549336>.
- Gu, D., and A. Gillespie. 1998. "Topographic Normalization of Landsat TM Images of Forest Based on Subpixel Sun-Canopy-Sensor Geometry." *Remote Sensing of Environment* 64 (2): 166–175. [https://doi.org/10.1016/S0034-4257\(97\)00177-6](https://doi.org/10.1016/S0034-4257(97)00177-6).
- Hantson, S., and E. Chuvieco. 2011. "Evaluation of Different Topographic Correction Methods for Landsat Imagery." *International Journal of Applied Earth Observation and Geoinformation* 13 (5): 691–700. <https://doi.org/10.1016/j.jag.2011.05.001>.
- Hu, Y., S. Wu, X. Feng, and L. Yang. 2020. "Topographic Correction of Leaf Area Index Product Derived from Remote Sensing Data." *Remote Sensing Technology and Application* 35 (5): 1070–1078. <https://doi.org/10.11873/j.issn.1004-0323.2020.5.1070>.
- Jiang, H., A. Chen, Y. Wu, C. Zhang, Z. Chi, M. Li, and X. Wang. 2022. "Vegetation Monitoring for Mountainous Regions Using a New Integrated Topographic Correction (ITC) of the SCS + C Correction and the Shadow-Eliminated Vegetation Index." *Remote Sensing* 14 (13): 3073. <https://doi.org/10.3390/rs14133073>.
- Jiang, H., S. Wang, X. Cao, C. Yang, Z. Zhang, and X. Wang. 2018. "A Shadow-Eliminated Vegetation Index (SEVI) for Removal of Self and Cast Shadow Effects on Vegetation in Rugged Terrains." *International Journal of Digital Earth* 12 (9): 1013–1029. <https://doi.org/10.1080/17538947.2018.1495770>.

- Li, A., Q. Wang, J. Bian, and G. Lei. 2015. "An Improved Physics-Based Model for Topographic Correction of Landsat TM Images." *Remote Sensing* 7 (5): 6296–6319. <https://doi.org/10.3390/rs70506296>.
- Li, H., L. Xu, H. Shen, and L. Zhang. 2016. "A General Variational Framework Considering Cast Shadows for the Topographic Correction of Remote Sensing Imagery." *ISPRS Journal of Photogrammetry & Remote Sensing* 117:161–171. <https://doi.org/10.1016/j.isprsjprs.2016.03.021>.
- Lin, X. W., J. G. Wen, S. B. Wu, D. L. Hao, Q. Xiao, and Q. H. Liu. 2020. "Advances in Topographic Correction Methods for Optical Remote Sensing Imageries." *Journal of Remote Sensing (Chinese)* 24 (8): 958–974. <https://doi.org/10.11834/jrs.20209167>.
- Ling, J., A. Li, and H. Jin. 2023. "Leaf Area Index Estimation Over Mountainous Areas by Coupling the DART Model and Random Forest." *Remote Sensing Technology and Application* 38 (1): 39–50. <https://doi.org/10.11873/j.issn.1004-0323.2023.1.0039>.
- Liu, S., X. Gu, H. Liang, F. Wei, Y. Dong. 2007. *MIPPR 2007: Remote Sensing and GIS Data Processing and Applications; and Innovative Multispectral Technology and Applications*. <https://doi.org/10.1117/12.750971>.
- Lu, X., S. Dong, H. Yan, T. Zhao, F. Zhao, and F. Xu. 2025. "Quantifying Global Vegetation Recovery Speed in Response to Extreme Drought Using Multi-Dimensional Spatiotemporal Data." *International Journal of Digital Earth* 18. 1. <https://doi.org/10.1080/17538947.2025.2507195>.
- Ma, Y., T. He, A. Li, and S. Li. 2021. "Evaluation and Intercomparison of Topographic Correction Methods Based on Landsat Images and Simulated Data." *Remote Sensing* 13 (20): 4120. <https://doi.org/10.3390/rs13204120>.
- Ma, Z., G. Jia, M. E. Schaepman, and H. Zhao. 2020. "Uncertainty Analysis for Topographic Correction of Hyperspectral Remote Sensing Images." *Remote Sensing* 12 (4): 705. <https://doi.org/10.3390/rs12040705>.
- Nath, B., and W. Ni-Meister. 2021. "The Interplay Between Canopy Structure and Topography and Its Impacts on Seasonal Variations in Surface Reflectance Patterns in the Boreal Region of Alaska—Implications for Surface Radiation Budget." *Remote Sensing* 13 (16): 3108. <https://doi.org/10.3390/rs13163108>.
- Nie, X., Z. Hu, Q. Zhu, and M. Ruan. 2021. "Research on Temporal and Spatial Resolution and the Driving Forces of Ecological Environment Quality in Coal Mining Areas Considering Topographic Correction." *Remote Sensing* 13 (14): 2815. <https://doi.org/10.3390/rs13142815>.
- Reeder, D. H. 2002. *Topographic Correction of Satellite Images: Theory and Application*. New Hampshire: Dartmouth College.
- Riano, D., E. Chuvieco, J. Salas, and I. Aguado. 2003. "Assessment of Different Topographic Corrections in Landsat-TM Data for Mapping Vegetation Types." *IEEE Transactions on Geoscience & Remote Sensing* 41 (5): 1056–1061. <https://doi.org/10.1109/TGRS.2003.811693>.
- Richter, R., T. Kellenberger, and H. Kaufmann. 2009. "Comparison of Topographic Correction Methods." *Remote Sensing* 1 (3): 184–196. <https://doi.org/10.3390/rs1030184>.
- Santini, F., and A. Palombo. 2019. "Physically Based Approach for Combined Atmospheric and Topographic Corrections." *Remote Sensing* 11 (10): 1218. <https://doi.org/10.3390/rs11101218>.
- Santini, F., and A. Palombo. 2022. "Impact of Topographic Correction on PRISMA, Sentinel-2, and Landsat 8 Images." *Remote Sensing* 14 (16): 3903. <https://doi.org/10.3390/rs14163903>.
- Soenen, S. A., D. R. Peddle, and C. A. Coburn. 2005. "SCS+C: A Modified Sun-Canopy-Sensor Topographic Correction in Forested Terrain." *IEEE Transactions on Geoscience & Remote Sensing* 43 (9): 2148–2159. <https://doi.org/10.1109/TGRS.2005.852480>.
- Teillet, P. M., B. Guindon, and D. G. Goodenough. 1982. "On the Slope-Aspect Correction of Multispectral Scanner Data." *Canadian Journal of Remote Sensing* 8 (2): 84–106. <https://doi.org/10.1080/07038992.1982.10855028>.
- Wu, Z., G. He, S. Huang, M. Wang, and J. Lin. 2017. "Terrain Effects Assessment on Remotely Sensed Fractional Vegetation Cover in Hilly Area of Southern China." *Journal of Remote Sensing* 21 (1): 159–167. <https://doi.org/10.11834/jrs.20176016>.
- Yan, H., J. Wang, X. Lu. 2023. "Effect and Applicability of Terrain Correction of Remote Sensing Images Based on Semi-Empirical Models." *Mountain Research* 2023 (5): 759–770. <https://doi.org/10.16089/j.cnki.1008-2786.000785>.

- Yao, H., B. Fu, W. Sun, Y. Zhou, Y. Wang, W. Jiang, H. He, Z. Chen, and Y. Song. 2025. "Quantifying Key Indicators of Essential Biodiversity Variables for Mangrove Species in Response to Hydro-Meteorological Factors." *International Journal of Applied Earth Observation and Geoinformation* 139:104535. <https://doi.org/10.1016/j.jag.2025.104535>.
- Yin, G., A. Li, S. Wu, W. Fan, Y. Zeng, K. Yan, B. Xu, J. Li, and Q. Liu. 2018. "PLC: A Simple and Semi-Physical Topographic Correction Method for Vegetation Canopies Based on Path Length Correction." *Remote Sensing of Environment* 215:184–198. <https://doi.org/10.1016/j.rse.2018.06.009>.
- Zhang, W., K. Li, F. Zhang, Y. Li, G. Yue, and J. Jiang. 2024. "Triple Shadow Multilinear Unmixing for Near-Ground Hyperspectral Vegetation Canopy Shadow Removal." *Computers and Electronics in Agriculture* 219:108815. <https://doi.org/10.1016/j.compag.2024.108815>.
- Zhou, Y., J. Chen, Q. Guo, R. Cao, and X. Zhu. 2014. "Restoration of Information Obscured by Mountainous Shadows Through Landsat TM/ETM+ Images Without the Use of DEM Data: A New Method." *IEEE Transactions on Geoscience & Remote Sensing* 52 (1): 313–328. <https://doi.org/10.1109/TGRS.2013.2239651>.
- Zhu, G., Y. Liu, W. Ju, and J. Chen. 2013. "Evaluation of Topographic Effects on Four Commonly Used Vegetation Indices." *Journal of Remote Sensing* 17 (1): 210–234. <https://doi.org/10.11834/jrs.20131380>.